Proper Frequencies of a Down-Looking Water-Vapor Radiometer Over Sea Surface

S. C. Wu
Tracking Systems and Applications Section

Altimeter observation on board an Earth-orbiting satellite (e.g., TOPEX) over sea surface is corrupted by, among others, the water vapor path delay. Such error can be calibrated for by a down-looking microwave radiometer. This article studies the effects of water vapor profile, sea surface temperature, wind speed and brightness temperature measurement error on the calibration precision. Proper frequency combinations are searched to minimize these effects.

I. Introduction

Tropospheric water vapor introduces path delay as large as 50 cm on radio propagation. The most effective calibration method has been that making use of passive microwave radiometers (Refs. 1-5). The thermal radiation of water vapor at frequencies near the 22.235-GHz water absorption line, which can be measured by a radiometer, is an accurate indication of water vapor content along the line of sight.

On a clear day when no cloud (liquid water droplets) is present, a ground-based single-frequency measurement of the sky brightness temperature is sufficient for the estimation of the water vapor content or the corresponding delay. When the line of sight passes through clouds, the observed brightness temperature increases rapidly even though the path delay is hardly affected. The cloud effect can be separated from the water vapor effect by making measurement at two different frequencies. Such separation is possible owing to the difference in radiation frequency spectra between water vapor and liquid water droplets.

Another factor affecting the accuracy of water vapor measurement is the variation of the water vapor vertical profile. This is due to the fact that the thermal radiation from an amount of tropospheric constituents (including water vapor) farther away from the radiometer is continuously attenuated (through absorption) by the nearer constituents along the line of sight; the same amount of water vapor at a different height will contribute to different brightness temperature at the radiometer. Such profile dependence can be alleviated by the selection of a proper frequency (Refs. 2, 6) or a combination of frequencies (Refs. 3, 7) for the radiometer.

When the measurement is made on board an aircraft or an Earth-orbiting satellite over a sea surface, the problem becomes more complicated than that of a ground-based measurement in two respects. First, the brightness temperature is now the combination of three components: the upward tropospheric radiation, the reflected downward tropospheric radiation and the sea surface radiation. Secondly, both the reflected and the radiated components by the sea surface are strongly dependent

on sea surface emissivity which in turn is a function of sea surface temperature and foam coverage. To achieve an accurate estimation of water vapor path delay, the variations of sea surface temperature and emissivity cannot be ignored.

In this article, we shall investigate whether sub-centimeter water-vapor delay is achievable using a down-looking radiometer with proper selection of two frequencies. The effects of vertical profile, sea surface temperature and wind speed (related to foam coverage), and brightness temperature measurement error will be studied. The absence of precipitation will be assumed.

II. Background

The quantity to be determined is the water vapor path delay (Ref. 8)

$$\Delta R = k \int_0^H \frac{\rho_v}{T} dh, \quad k = 1.723 \times 10^{-3}\ K/(g/m^3) \qquad (1)$$

where ρ_v is the water vapor density and T is the atmospheric temperature along the vertical ray path h; H is the altitude of the radiometer. The quantity which is measured by a radiometer is the brightness temperature

$$T_B = \int_0^H T\alpha \exp\left(-\int_h^H \alpha dh\right) dh + e^{-\tau}\left[\epsilon_s T_s + (1-\epsilon_s)\left(\int_0^H T\alpha \exp\left(-\int_0^h \alpha dh\right) dh + T_c\, e^{-\tau}\right)\right] \qquad (2)$$

Here, the first term is due to the upward tropospheric radiation; the terms in the brackets are due to the sea surface radiation and the sea surface reflections of the downward tropospheric radiation and of the cosmic radiation. These bracketed terms are attenuated by the tropospheric absorption $\tau = \int_0^H \alpha\, dh$, with $\alpha = \alpha_v + \alpha_c + \alpha_o$ being the combined absorption coefficient of water vapor, cloud and oxygen along the ray path. The sea surface emissivity is denoted by ϵ_s and the sea surface temperature by T_s. The cosmic radiation has a value of $T_c \doteqdot 2.9$ K. From Eq. (2) the dependence of T_B on ϵ_s, T_s and the vertical profile of α may be appreciated.

To measure the water vapor path delay by a radiometer a calibration equation relating the two quantities, ΔR in (1) and T_B in (2), needs to be established.

III. Calibration Equation

The brightness temperature of Eq. (2) can be expressed as the following approximation (Ref. 9: In Ref. 9 the cosmic radiation T_c has been omitted):

$$T_B \doteqdot T_e + e^{-\tau}\epsilon_s(T_s - T_e) - e^{-2\tau}(1-\epsilon_s)(T_e - T_c) \qquad (3)$$

where T_e is the effective temperature defined as

$$T_e = \frac{\int_0^H T\alpha \exp\left(-\int_h^H \alpha dh\right) dh}{\int_0^H \alpha \exp\left(-\int_h^H \alpha dh\right) dh} \qquad (4)$$

The absorption τ, which is the algebraic sum of the contributions from water vapor, cloud and oxygen, increases *linearly* with the amount of water vapor content along the ray path. Hence it is the logical quantity to be related to ΔR. Solving for τ from (3) we have

$$\tau = \ln\left[\frac{2(1-\epsilon_s)(T_e - T_c)}{\epsilon_s(T_s - T_e) + \sqrt{\epsilon_s^2(T_s - T_e)^2 + 4(1-\epsilon_s)(T_e - T_c)(T_e - T_B)}}\right] \qquad (5)$$

In the calculation of τ using (5), the effective temperature T_e needs to be accurately estimated. To loosen the dependence on the estimation of T_e, a quantity $T_e^\gamma\, \tau$ is to be used instead of τ. The exponent γ is selected such that $T_e^\gamma\, \tau$ is insensitive to the variation of T_e. In other words, $\partial(T_e^\gamma\, \tau)/\partial T_e = 0$. The derivative is rather lengthy but straightforward. After calculating the derivative and using the typical values $T_s = 290$ K, $T_e = 275$ K, $T_B = 150$ K and $\epsilon_s = 0.45$ we have $\gamma \doteqdot 2$. Therefore, $T_e^2\, \tau$ is to be used as the parameter in the calibration equation.

It can be numerically shown that

$$T_e^2\, \tau \doteqdot \int_0^H T^2\, \alpha dh$$

or

$$T_e^2\, \tau \doteqdot \int_0^H T^2(\alpha_v + \alpha_c + \alpha_o)\, dh \qquad (6)$$

Since α_c is proportional to f^2 (Ref. 10) for microwave frequencies $f < 40$ GHz, it can be eliminated for a dual-frequency radiometer:

$$\frac{(T_e^2\,\tau)_1}{f_1^2} - \frac{(T_e^2\,\tau)_2}{f_2^2} = \int_0^H w(h)\,\frac{\rho_v}{T}\,dh + T_{ox}^2 \quad (7)$$

where

$$w(h) = \frac{T^3}{\rho_v}\left(\frac{\alpha_{v,1}}{f_1^2} - \frac{\alpha_{v,2}}{f_2^2}\right) \quad (8)$$

and

$$T_{ox}^2 = \int_0^H T^2\left(\frac{\alpha_{o,1}}{f_1^2} - \frac{\alpha_{o,2}}{f_2^2}\right)dh \quad (9)$$

A comparison of (1) and (7) indicates that a linear relationship between ΔR and $T_e^2\tau$ at the two frequencies can be established provided the weighting function $w(h)$ be a constant, independent of h. Under such circumstances,

$$\Delta R = a_0 + a_1(T_e^2\tau)_1 + a_2(T_e^2\tau)_2 \quad (10)$$

where the constant coefficients are

$$a_0 = \frac{-k}{w}T_{ox}^2$$

$$a_1 = \frac{k}{wf_1^2} \quad (11)$$

$$a_2 = \frac{-k}{wf_2^2}$$

For $f < 40$ GHz, the oxygen absorption coefficient α_o also increases with approximately f^2. Hence T_{ox}^2 as defined by (9) is a small residual oxygen effect. Furthermore, α_o is proportional to $T^{-2.85}$ (Ref. 11); $T^2\alpha_o$ is insensitive to the temperature T. Therefore, T_{ox}^2 is practically a constant. Note that a constant $w(h)$ implies the estimation of ΔR being independent of the water vapor vertical profile. In the following section, frequency pairs for which $w(h)$ remains nearly constant will be searched.

IV. Frequency Pairs for Constant $w(h)$

The procedure of Ref. 7 is to be followed in the search for frequency pairs resulting in nearly constant $w(h)$. In brief, the single frequency contributions of $w(h)$ in (8) are calculated and plotted on the same graph, as depicted by Fig. 1; any pair (e.g., b and c in Fig. 1) having a wide and nearly constant separation will result in a large and constant $w(h)$ and can be selected as a candidate for further consideration. The actual calculation will be based on the radiosonde measurements of the meteorology profiles at Point Mugu, California, on February 24, 1976. These profiles are shown in Fig. 2. It has been shown in Ref. 7 that, for a ground-based radiometer with specified frequencies, the shape of $w(h)$ vs h is similar for different profile shapes. Since the form of $w(h)$ in (8) differs only by a multiplicative factor T which normally has a small fractional variation, the same can be said for a down-looking radiometer. Hence the profile of Fig. 2 and the resulting $w(h)$ can be considered as typical. Note that we need to examine $w(h)$ only for h below about 5 km since there is little water vapor content at higher altitudes.

Figure 3 shows the components of $w(h)$ for frequencies near the 22.235-GHz water absorption line. Two of the pairs having wide and nearly constant separations are found to be 20.2 GHz/26.0 GHz and 24.3 GHz/32.0 GHz. The normalized variations in $w(h)$ of these frequency pairs are shown in Fig. 4. Also shown are the 20.3 GHz/31.4 GHz optimum pair for a ground-based radiometer (Ref. 7), the 22.235 GHz/31.4 GHz pair selected by the Nimbus-6 Scanning Microwave Spectrometer (SCAMS) (Ref. 9) and the pair 18.0 GHz/21.0 GHz believed to be insensitive to sea surface temperature[1]. Note that the last two pairs have large $w(h)$ variations. The pair for the optimum ground-based radiometer (20.3 GHz/31.4 GHz) is only slightly inferior to the remaining two at higher altitudes. The pair with least variation in $w(h)$ is found to be 24.3 GHz/32.0 GHz.

The values of T_{ox}^2 in (9) and of $w(h)$ in (8) at sea surface ($h = 0$) are calculated and shown in Table 1. The 24.3 GHz/32.0 GHz pair not only has a reasonably large $w(0)$ for small sensitivity to $T_e^2\tau$ error when (10) is used to estimate the water vapor path delay, it also has the lowest T_{ox}^2, which implies being least affected by the variation in the residual oxygen term.

V. Effects of Sea Surface Temperature and Wind Speed

The variation in sea surface temperature affects the estimation of the water vapor path delay in two respects. First, it varies the values of the weighting function w, which in turn varies the calibration equation coefficients (cf. Eq. 11). Secondly, it varies the observable $T_e^2\tau$ through T_s and ϵ_s (cf.

[1] T. Chester, private communication.

Eq. 5). The variation in sea surface wind speed has an effect only through ϵ_s.

To study the effect of sea surface temperature and wind speed through ϵ_s, it is convenient to work out an empirical mathematical expression for ϵ_s in terms of f, T_s and V_w, the sea surface wind speed. Figure 5 shows the frequency dependence of ϵ_s at T = 293 K (Ref. 12). The effect of sea water salinity is found to be negligibly small for $f > 5$ GHz. The area which concerns us is the nadir ray path in the frequency range of 15 to 35 GHz. Within this range ϵ_s is nearly linear in frequency and can be represented by

$$\epsilon \doteqdot 0.34(1 + 0.01f), \quad T = 293 \text{ K} \tag{12}$$

The temperature dependence of ϵ_s can be derived from Fig. 6 (Ref. 12), where the change in $T_s\epsilon_s$ per change in T_s as a function of f is shown. This figure applies to the temperature range of 273 to 303 K, practically all possible sea surface temperatures. Over the frequency range of interest, a close approximate expression for the nadir observation is

$$\frac{\Delta(T_s\epsilon_s)}{\Delta T_s} \doteqdot 1.46\, e^{-0.04f} - 0.64 \tag{13}$$

Wind over the sea surface increases the emissivity through the amount of foam coverage. Nordberg et al. (Ref. 13) found that, at f = 19.35 GHz, there is no detectable effect for wind speeds less than 7 m/sec while $T_s\epsilon_s$ increases by 1 K per m/sec above that, as shown in Fig. 7. The effect is nearly frequency-independent, as has been discovered by Webster et al. (Ref. 14), in the frequency range we are concerned with. This is shown in Fig. 8. The effect of wind speed can be expressed as

$$\frac{\partial(T_s\epsilon_s)}{\partial V_w} \doteqdot \delta_{-1}(V_w - 7) \tag{14}$$

where $\delta_{-1}(x)$ is the unit step function defined by

$$\delta_{-1}(x) = \begin{cases} 0 \ , & x < 0 \\ 1 \ , & x \geqslant 0 \end{cases}$$

Combining (12), (13) and (14) we arrive at the following empirical expression for the sea surface emissivity:

$$\epsilon_s = \frac{99}{T_s}(1 + 0.01f) + \left(\frac{T_s - 293}{T_s}\right)(1.46\, e^{-0.04f} - 0.64)$$

$$+ \delta_{-2}(V_w - 7)/T_s \tag{15}$$

where $\delta_{-2}(x)$ is the unit ramp function defined by

$$\delta_{-2}(x) = \begin{cases} 0 \ , & x < 0 \\ x \ , & x \geqslant 0 \end{cases} \tag{16}$$

The sea surface value of the weighting function, $w(0)$, varies with the surface values of T^3 and α_v/ρ_v (cf. Eq. 8). The variation in α_v/ρ_v is small as compared to that in T^3. Hence it is a good approximation to assume $w(0)$ as being dependent only on T in the form

$$w(0) \propto T_s^3 \tag{17}$$

VI. Numerical Results

In this section, we shall study the statistical uncertainty in the estimation of water vapor path delay using the calibration equation (10) with different frequency pairs. Five sets of theoretical coefficients are calculated from the values of T_{ox}^2 and $w(0)$ in Table 1 of the typical meteorology profiles in Fig. 2.

The test data are a set of 75 meteorology soundings derived from expanding 25 measurements at Point Mugu, California, from February 24 to March 17, 1976. The expansion is furnished by simply adding -10 K and 10 K to the temperature profiles, to simulate the worldwide coverage of temperature range. The brightness temperatures that would be measured by a radiometer are calculated by (2). The measurements cover all altitudes up to ~10 km, above which the water vapor content is rare. These data are extrapolated to an altitude at which the total pressure drops to 100 mbar ($H \doteqdot 16$ km) to include ~99% of the oxygen contribution to T_B.

The theoretical coefficients derived from Table 1 and the brightness temperatures calculated from the 75 soundings are used to estimate the water vapor path delay by Eq. (10). The effective temperature T_e is found to be ~0.95 T_s for all frequencies. The estimated ΔR are to be compared with the actual ΔR calculated from (1). The statistics of their differences provide an estimate of the calibration equation uncertainty.

Four different test cases are to be studied:

Case 1: No wind ($V_w < 7$ m/sec)
Coefficients scaled by T_s^{-3}
τ calculated by correct T_s

Case 2: No wind
Coefficients fixed
τ calculated by fixed T_s (287.6 K from Fig. 2)

Case 3: 10 ± 5 m/sec wind
Coefficients scaled by T_s^{-3}
τ calculated by V_w = 10 m/sec and correct T_s

Case 4: 10 ± 5 m/sec wind
Coefficients fixed
τ calculated by V_w = 10 m/sec and T_s = 287.6 K

Table 2 summarizes the results of the comparison. The following points are observed:

(1) When independent measurements of sea surface temperature and wind speed are available and are applied to the calculations of τ and the calibration coefficients (Case 1), the uncertainties are less than 1 cm for all five frequency pairs.[2] The three having nearly constant $w(h)$ in Fig. 4 are 3-5 times better than the remaining two. This verifies the reduction of profile dependence of Eq. (10) with proper frequency pairs.

(2) When sea surface temperatures (having a standard deviation σ_{T_S} = 9.2 K) are not independently measured (Case 2), the uncertainties increase by an appreciable amount for the first four frequency pairs. The pair 18 GHz/21 GHz is nearly unchanged. Such insensitivity to sea surface temperature is a result of compensation between the change in w and the change in $T_e^2\tau$ due to a change in T_s.

(3) When the sea surface wind speed is mismodeled by σ_{v_W} = 5 m/sec (Case 3), the uncertainties in ΔR increase by 0.8 - 1.4 cm. The pair 20.3 GHz/31.4 GHz has the largest increase and the pair 22.235 GHz/31.4 GHz has the least.

(4) When the mismodeling includes both σ_{v_W} = 5 m/sec and σ_{T_S} = 9.2 K (Case 4), the combined effects are nearly the RSS of the two separate effects. The frequency pair having the most constant $w(h)$ – 24.3 GHz/32.0 GHz – is still better than the other four, with an uncertainty of ~1.5 cm.

The uncertainties above have been estimated using theoretical coefficients in the calibration equation (10). These uncertainties would have been lower had the coefficients been derived from regression analysis with the 75 soundings. For comparison, these estimates are summarized in Table 3. It is believed that such "forced-fitting" may result in an optimistic estimate. An ideal error estimation approach would be such that the calibration coefficients are derived from a regression analysis with one set of data and are applied to another set of data for ΔR error estimation.

Another error source not included in the above analysis is in the brightness temperature measurement. The sensitivity to such error can be estimated by omitting the term containing $e^{-\tau}$ in (3) and then substituting into (10) and taking partial derivative with respect to T_B:

$$\frac{\partial(\Delta R)}{\partial T_{B,i}} = a_i T_e^2 \frac{\partial \tau_i}{\partial T_{B,i}} \qquad i = 1, 2$$

$$\doteq \frac{\pm k\, T_e^2}{2wf_i^2} / (T_e - T_{B,i}) \,, \quad \begin{matrix} + \text{ for } i = 1 \\ - \text{ for } i = 2 \end{matrix} \tag{18}$$

Hence, the sensitivity is small for large wf_i^2 and small $T_{B,i}$ (well below saturation). For the typical meteorology profiles of Fig. 2, the sensitivities are calculated and summarized in Table 4. The frequency pair 22.235 GHz/31.4 GHz has the lowest sensitivity, as expected for its large w (cf. Table 1). The pair 18.0 GHz/21.0 GHz has a sensitivity a factor of 3 larger.

VII. Conclusions

The analysis indicates that it is possible to achieve a subcentimeter estimate of water vapor path delay on nadir observation with an on-board microwave radiometer. To achieve such precision we need (1) a radiometer with two properly selected frequencies, (2) brightness temperature measurement accurate to ~0.5 K, (3) knowledge of sea surface temperature to ~3 K and (4) knowledge of sea surface wind speed to ~2 m/sec or knowledge of sea surface emissivity to ~0.01. Note that the analysis does not apply when there is precipitation.

The frequency pair 24.3 GHz/32.0 GHz is found to be ideal for a nadir water vapor radiometer. It is insensitive to profile variation and has a moderate sensitivity to brightness temperature measurement error.

The frequency pair 18.0 GHz/21.0 GHz, though insensitive to sea surface temperature uncertainty, has high sensitivities to profile variation and to brightness temperature measurement error. It can be considered only when no knowledge of sea surface temperature is available and the brightness temperature measurement error is highly correlated (and thus cancelled) between the two frequencies.

[2] The large biases for the last two frequency pairs are due to an underestimate of w by the surface values. Such biases can be reduced by using w at an altitude above sea surface for the calculation of coefficients in (11).

References

1. Barrett, A. H., and Chung, V. K., "A Method for the Determination of High-Altitude Water-Vapor Abundance from Ground-Based Microwave Observations," *J. Geophys. Res.*, Vol. 67, No. 11, pp. 4259-4266, 1962.

2. Westwater, E. R., "An Analysis of the Correction of Range Errors Due to Atmospheric Refraction by Microwave Radiometric Techniques," Tech. Rep. IER 30-ITSA 30, Environmental Science Services Administration, U.S. Dept. of Commerce, Boulder, CO, 1967.

3. Gaut, N. E., "Study of Atmospheric Water Vapor by Means of Passive Microwave Techniques," Tech. Rep. 467, MIT Res. Lab. of Electronics, Dec. 20, 1968.

4. Schaper, L. W., Jr., Staelin, D. H., and Waters, J. W., "The Estimation of Tropospheric Electrical Path Length by Microwave Radiometry," *Proc. IEEE*, Vol. 58, No. 2, pp. 272-273, 1970.

5. Decker, M. T., Guiraud, F. O., and Westwater, E. R., "Correction of Electrical Path Length by Passive Microwave Radiometry," in *Proc. Conf. on Propagation of Radio Waves at Frequencies above 10 GHz*, London, England, April 10-13, 1973.

6. Menius, A. C., Martin, C. F., Layson, W. M., and Flagg, R. S., "Tropospheric Refraction Corrections Using a Microwave Radiometer," Tech. Staff Tech. Memo, 19 ETV-TM-64-12, Pan American Airways, Nov. 16, 1964.

7. Wu, S. C., "Optimum Frequencies of a Passive Microwave Radiometer for Tropospheric Path-Length Correction," *IEEE Trans. Ant. Prop.*, Vol. AP-27, No. 2., pp. 233-239, March 1979.

8. Bean, B. R., and Dutton, E. J., *Radio Meteorology*, National Bureau of Standards Monograph 92, Boulder, CO, 1966.

9. Grody, N. C., Gruber, A., and Shen, W. C., "Atmospheric Water Content Over the Tropical Pacific Derived from the Nimbus-6 Scanning Microwave Spectrometer," *J. Appl. Meteorology*, Vol. 19, pp. 986-996, August 1980.

10. Staelin, D. H., "Measurements and Interpretation of the Microwave Spectrum of the Terrestrial Atmosphere near 1-Centimeter Wavelength," *J. Geophys. Res.*, Vol. 71, No. 12, pp. 2875-2881, 1966.

11. Van Vleck, J. H., Purcell, E. M., and Goldstein, H., "Atmospheric Attenuation", in *Propagation of Short Radio Waves*, D. E. Kerr, ed., McGraw-Hill, Chapter 8, 1951.

12. Wilheit, T. T., Jr., "A Review of Applications of Microwave Radiometry to Oceanography," *Boundary-Layer Meteorology*, Vol. 13, pp. 277-293, 1978.

13. Nordberg, W., Conaway, J., Ross, D. B., and Wilheit, T., "Measurements of Microwave Emission from a Foam-Covered Wind Driven Sea," *J. Atmos. Sci.*, Vol. 28, pp. 429-435, 1971.

14. Webster, W. J., Jr., Wilheit, T. T., Ross, D. B., and Gloersen, P., "Spectral Characteristics of the Microwave Emission from a Wind-Driven Foam-Covered Sea," *J. Geophys. Res.*, Vol. 81, No. 18, pp. 3095-3099, June 1976.

Table 1. Values of $T_{OX}2$ and $w(0)$ for typical meteorology profiles

f_1	20.2 GHz	24.3 GHz	20.3 GHz	22.235 GHz	18.0 GHz
f_2	26.0 GHz	32.0 GHz	31.4 GHz	31.4 GHz	21.0 GHz
T_{ox}^2	0.579	0.189	0.659	0.394	0.565
$10^3\ w(0)$	1.03	1.11	1.60	1.89	0.99

Table 2. Calibration uncertainty of ΔR (cm) using theoretical coefficients derived from Table 1

f_1	20.2 GHz	24.3 GHz	20.3 GHz	22.235 GHz	18.0 GHz
f_2	26.0 GHz	32.0 GHz	31.4 GHz	31.4 GHz	21.0 GHz
Case 1	−0.06 ± 0.15	−0.24 ± 0.18	−0.26 ± 0.18	1.19 ± 0.64	1.72 ± 0.77
Case 2	−0.07 ± 1.44	−0.26 ± 0.98	−0.28 ± 1.25	1.19 ± 1.39	1.71 ± 0.80
Case 3	−0.06 ± 1.16	0.16 ± 1.13	0.28 ± 1.49	1.36 ± 1.06	1.39 ± 1.32
Case 4	−0.07 ± 1.94	0.13 ± 1.43	0.25 ± 1.85	1.37 ± 1.67	1.36 ± 1.43

Table 3. Calibration uncertainty of ΔR (cm) using regression coefficients derived from forced-fitting ΔR and the simulated τ through Eq. (10)

f_1	20.2 GHz	24.3 GHz	20.3 GHz	22.235 GHz	18.0 GHz
f_2	26.0 GHz	32.0 GHz	31.4 GHz	31.4 GHz	21.0 GHz
Case 1	0.00 ± 0.15	0.00 ± 0.15	0.00 ± 0.15	−0.02 ± 0.47	−0.02 ± 0.45
Case 2	0.00 ± 1.32	0.00 ± 0.96	0.00 ± 1.19	0.00 ± 1.13	0.00 ± 0.51
Case 3	0.00 ± 0.99	0.01 ± 1.07	−0.02 ± 1.21	−0.01 ± 0.71	0.01 ± 0.92
Case 4	0.00 ± 1.54	0.00 ± 1.31	0.00 ± 1.67	0.00 ± 1.22	0.00 ± 0.98

Table 4. ΔR sensitivity to T_B measurement error

f_1	20.2 GHz	24.3 GHz	20.3 GHz	22.235 GHz	18.0 GHz
f_2	26.0 GHz	32.0 GHz	31.4 GHz	31.4 GHz	21.0 GHz
$\frac{\partial(\Delta R)}{\partial T_{B,1}}$	1.17	0.79	0.75	0.57	−1.42
$\frac{\partial(\Delta R)}{\partial T_{B,2}}$	−0.73	−0.47	−0.34	−0.29	1.16
Worst case	1.90	1.26	1.09	0.86	2.58

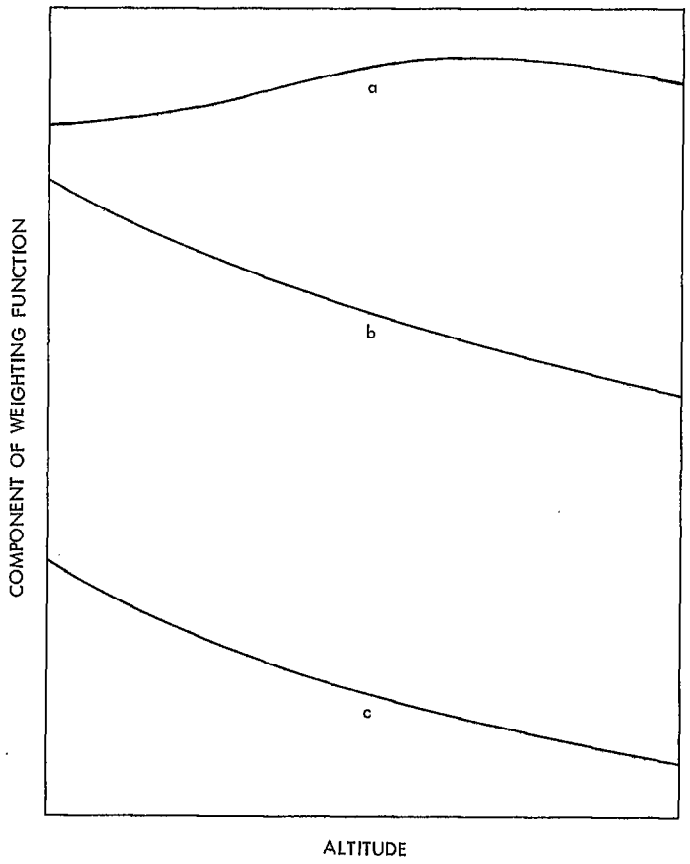

Fig. 1. Descriptive examples of weighting function components at three different frequencies; the pair combining b and c has a constant separation and will result in a constant weighting function

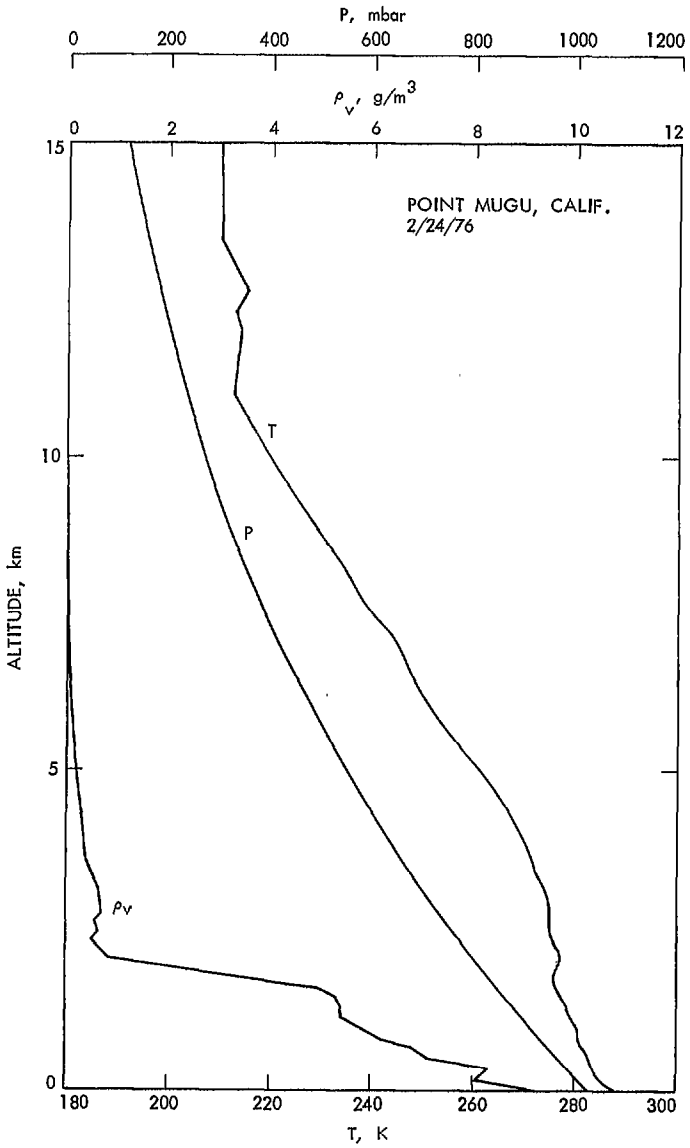

Fig. 2. Typical profiles of atmospheric temperature, pressure and water-vapor density

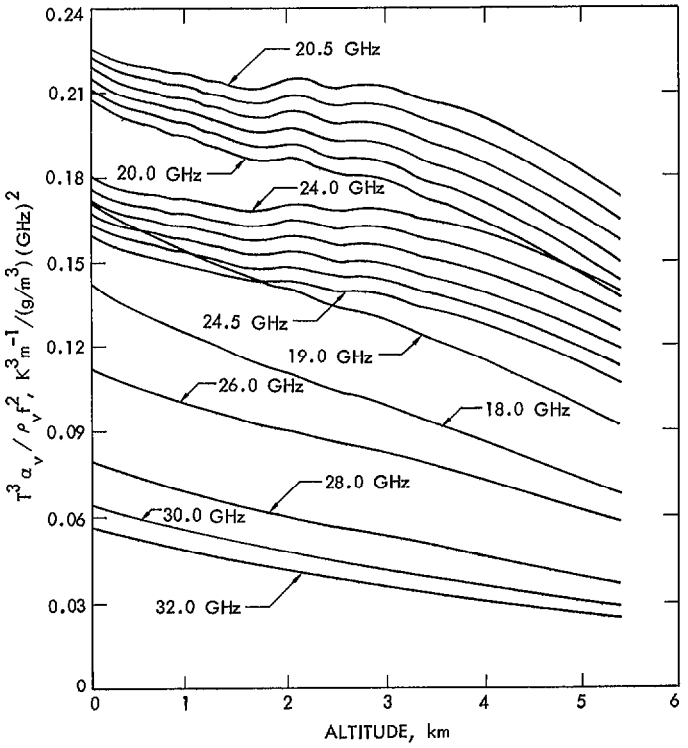

Fig. 3. Components of weighting functions for various frequencies

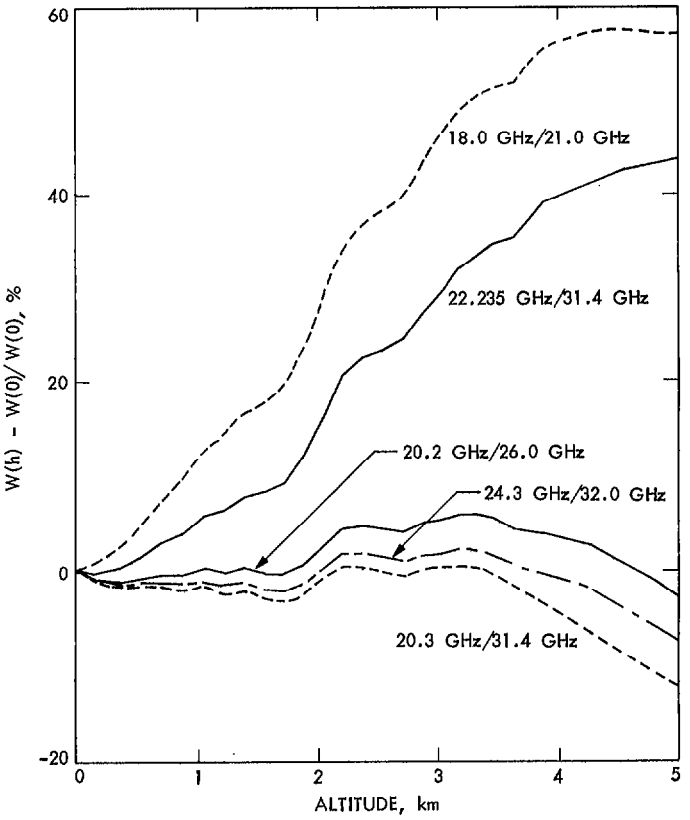

Fig. 4. Normalized weighting functions for various frequency pairs

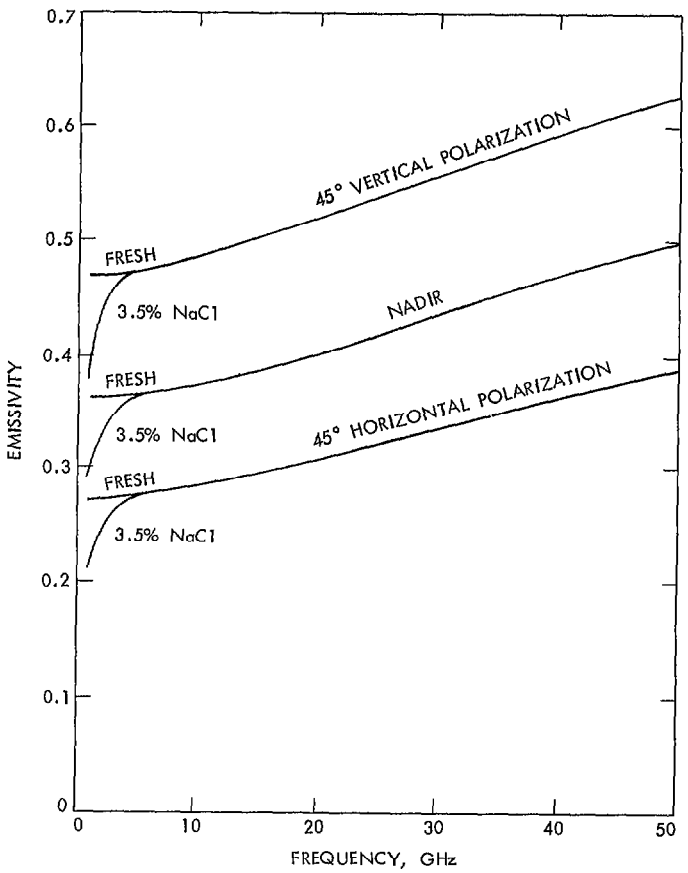

Fig. 5. Emissivity of water at temperature T_S = 290 K (from Ref. 12)

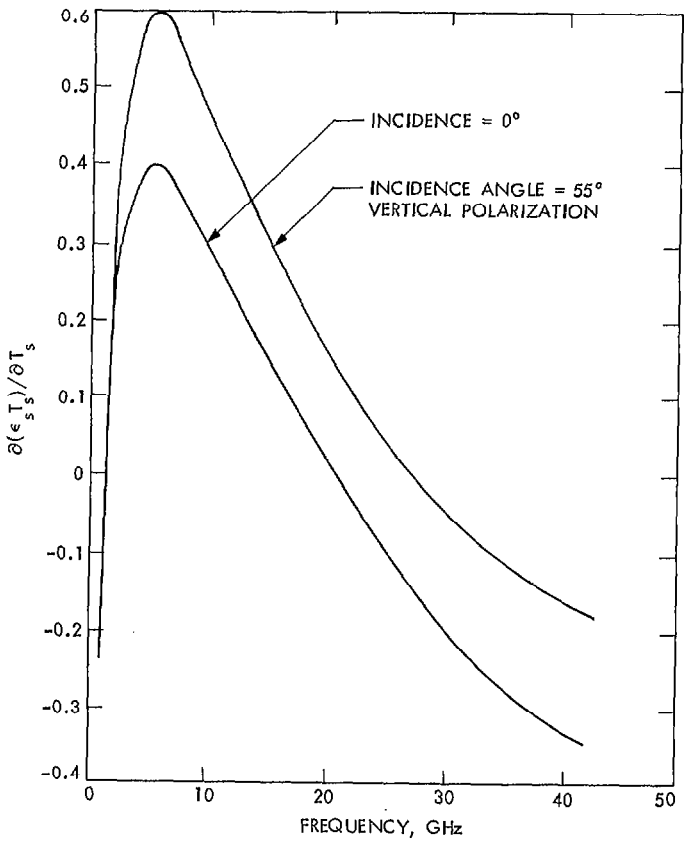

Fig. 6. Change of sea surface emission ($\epsilon_S T_S$) per change of sea surface temperature (T_S) as a function of frequency (from Ref. 12)

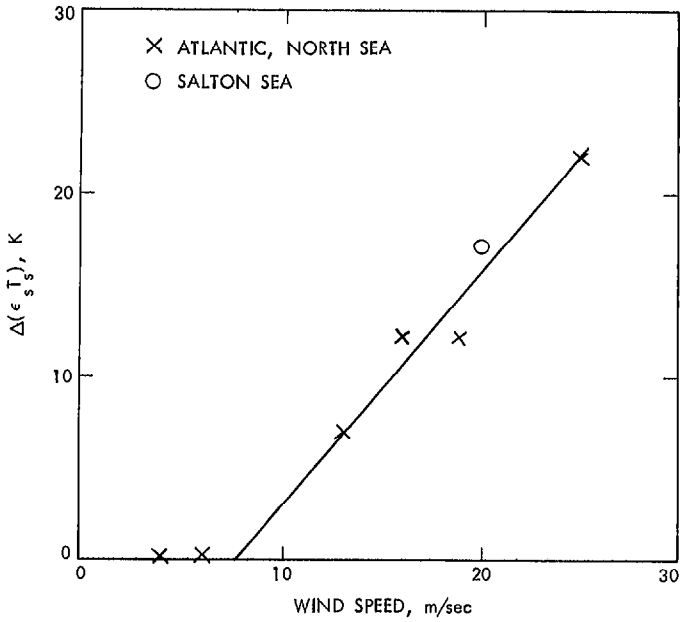

Fig. 7. Increase of $\epsilon_S T_S$ at 19.35 GHz caused by wind speed at sea surface (from Ref. 13)

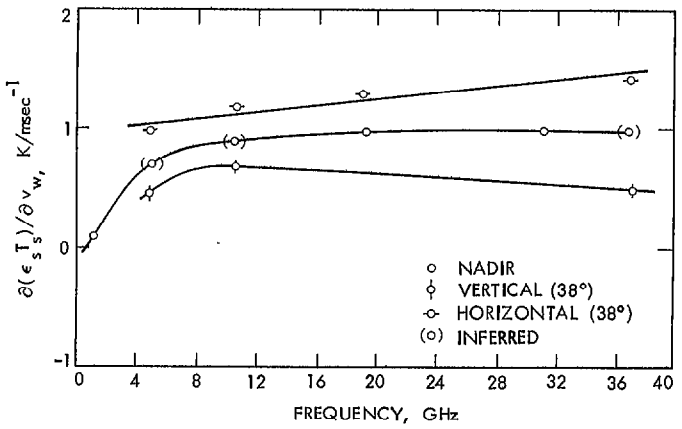

Fig. 8. Rate of increase of $\epsilon_S T_S$ with wind speed as a function of frequency (from Ref. 14)